APPLICATION OF FUNDAMENTAL STRUCTURAL MECHANICS PRINCIPLES IN ASSESSING THE CARDINGTON RESTRAINED BEAM TEST

A.S.Usmani
School of Civil and Environmental Engineering, University of Edinburgh

Keywords: Simple analytical model, Cardington fire tests, structural behaviour in fire.

Abstract

The understanding of the fundamental principles of mechanics that govern the behaviour of structures subjected to thermal actions is vital to the understanding the behaviour of composite frame structures (like the Cardington frame) in fire. A set of basic principles have been developed and presented in various reports and presentations, and form one of a number of important outputs from the PIT project, sponsored by DETR (UK). The PIT project was about developing computational models of the full-scale fire tests on the steel frame at Cardington (UK). However in executing this massive computational exercise properly, and interpreting the voluminous results from the many computational models developed, it was found necessary, time and again, to go back to the basics and develop the appropriate theory. It will be shown that these principles not only provide a good basis for checking the qualitative accuracy of the results, but also provide a reasonable order-of-magnitude type quantitative prediction of the key measures of structural behaviour. Such an analysis is an enormously practical and powerful tool to allow engineers to make quick preliminary calculations for real life engineering problems and also provides a means to check results from large and complex numerical models to ensure that they are consistent with the basic principles.

1 Introduction

This paper builds upon earlier work presented at the INTERFLAM and SiF conferences [1, 2]. These papers presented some of the fundamental principles of structural mechanics that govern the behaviour of steel framed composite structures in fire, such as the one at BRE LBTF at Cardington (Bedfordshire, UK). It has been shown by the work undertaken as part of the DETR PIT project [3] that the response of steel frame composite structures in fire is dominated by the thermal effects. The main message from this project was that for realistic fire scenarios in real structures, the behaviour is governed much more by the manner in which the structure accommodates the thermally induced strains, and much less so by the conventional parameters of loads and material strength which are dominant at ambient temperatures. A large variety of internal force and displacement combinations exist based upon the thermally induced expansions and curvatures and the structural restraints to these imposed strains as presented in [4]. The objective of this paper is to use the principles presented in this paper in a practical manner to develop A simple model of the Cardington restrained beam test and assessing the results in a qualitative and quantitative manner against more sophisticated FEM computational analyses.

A summary of the main principles outlined in [4] is as follows:

1 Unrestrained thermal expansion caused by a rise in mean temperature causes ends to move apart. The thermal strain producing this expansion is

$$\varepsilon_T = \alpha \Delta T$$

where α is the coefficient of thermal expansion and ΔT is the average temperature increment.

2 Thermal expansion in the presence of restraint to lateral translation from the surrounding structure produces compression forces leading to yielding or buckling (both the restraint and the temperature rise do not have to be large for buckling or yielding to occur).

3 Thermal bowing caused by the through depth thermal gradient leads to curvature,

$$\phi = \alpha T_{,z}$$

where $T_{,z}$ is the average temperature gradient through the beam depth. The thermally induced curvature results in the pulling in of the ends in a simply supported beam. The reduction in distance between the ends is written as a "contraction" strain,

$$\varepsilon_{\phi} = 1 - \frac{\sin\frac{l\phi}{2}}{\frac{l\phi}{2}}$$

where, l is the length of the beam.

4 Restraint to end translation produces tensions in the beam which grow with growth in thermal gradients.

5 Rigid restraint to end rotation produces a hogging moment of $EI\phi$ over the whole length of the beam with no curvature. Finite rotational restraints produce combinations of hogging moments and curvature.

6 Compatibility of displacements in compartments with orthogonal stiffness distribution and orthogonal temperature distribution (for instance, steel only in one direction) influences the forces and displacements in the members.

2 Assessment of the restrained beam test

Figure 1 shows the structural layout and compartment location for the British Steel restrained beam test at Cardington. The compartment is highly rectangular and also highly restrained. The reinforced concrete deck and steel secondary beam act compositely in the longitudinal direction as shown in Figure 1. In the transverse direction the profiled RC slab with the steel decking bridges the load between secondary beams. Figure 2 shows the effective structural sections that will be active, if the composite slab were to be idealised in the manner of a grillage. This is not a bad idealisation as the flexural stiffness of the slab in the transverse direction is an order of magnitude higher than its stiffness in the longitudinal direction. For the approximate analysis to be undertaken here, three different situations during the test will be considered for the purpose of illustration. However the calculations and procedures used can be refined much further if so desired. The cases to be considered are; a) Low compartment temperatures with unprotected steel sections assumed fully active; b) Moderate temperatures with unprotected steel properties reduced considerably; c) High compartment temperatures with unprotected steel properties assumed to be zero. The properties of the sections used are as given in Table 1.

2.1 Estimation of restraints and simple analytical model

Upon heating, the steel beam begins to expand against the restraint provided by beams in the adjacent cold compartment. There are two effects of heating, the steel section expands and develops large internal compression forces and the composite longitudinal section begins to acquire a thermally induced curvature (*thermal bowing*) due to the difference between the steel and concrete

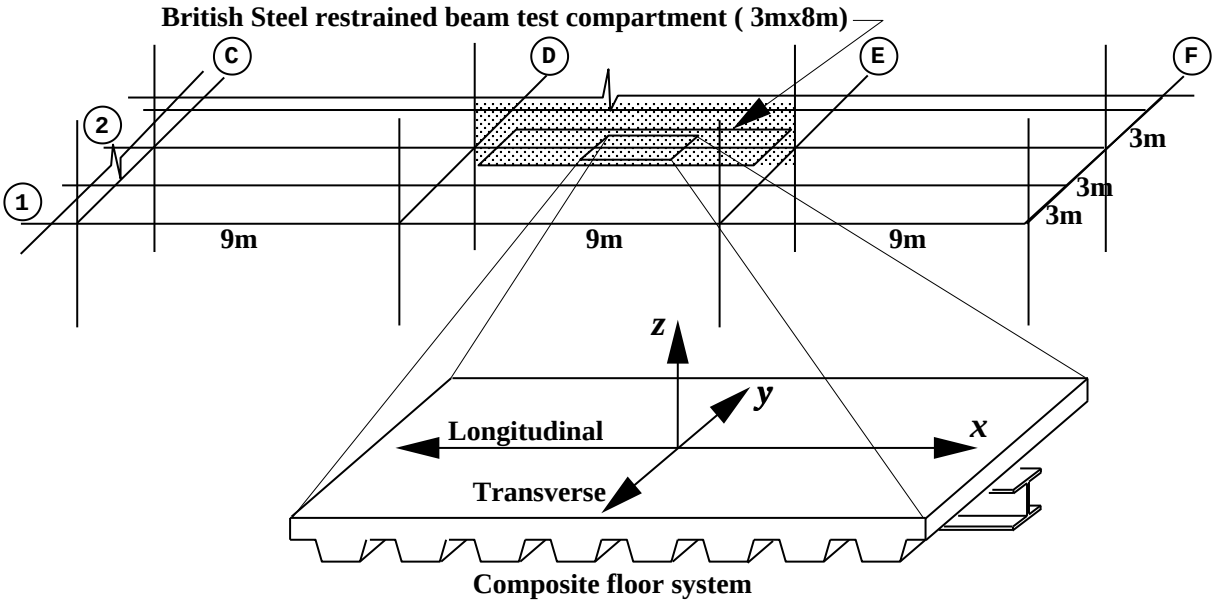

Figure 1: Layout of the restrained beam test at Cardington

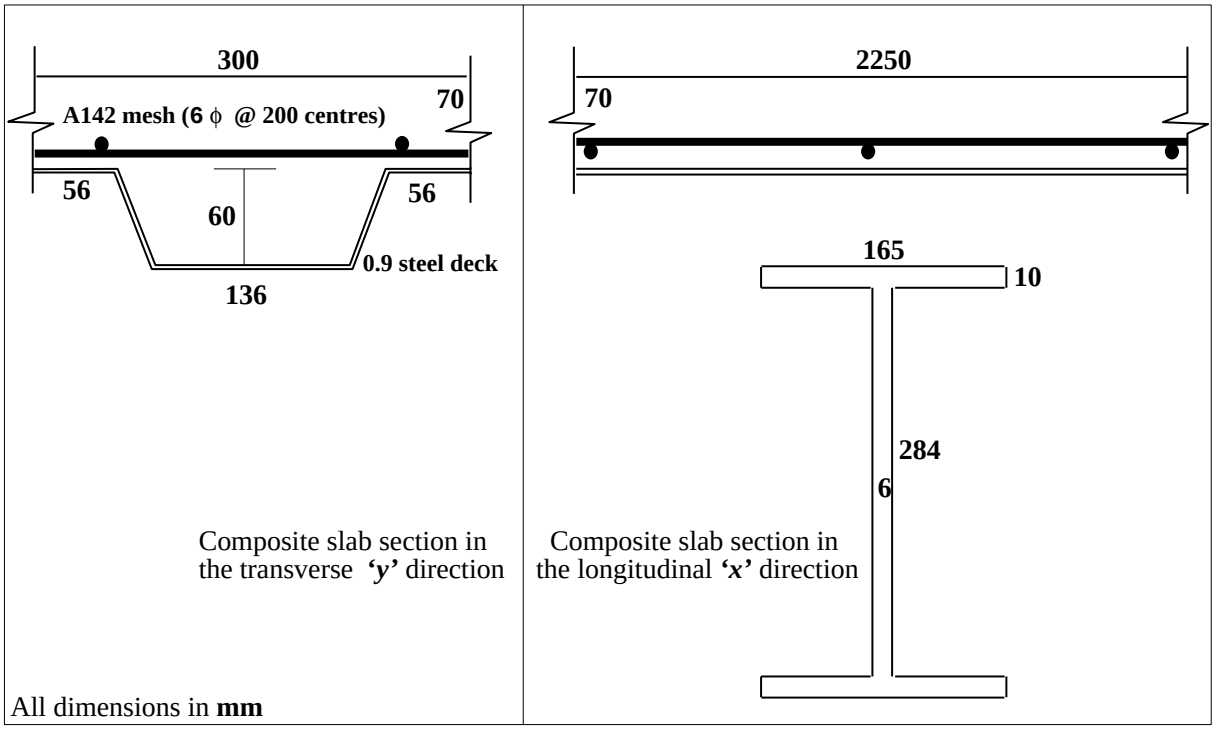

Figure 2: Active composite cross-sections in x and y directions

	Area	2nd Moment	Centroid depth	Modulus	Thermal expansion coef.
	$(A)\,\mathrm{mm}^2$	$(I)\,\mathrm{mm}^4$	$(\bar{y})$ mm	$(E)\,\mathrm{kN/mm}^2$	$(\alpha)\,/^\circ\mathrm{C}$
x-Slab	157500	257×10^6	35	7.5	8.0×10^{-6}
Steel beam	5150	85×10^6	282	200	12.0×10^{-6}
x-Composite	10900	250×10^6	148	200	10.0×10^{-6}
y-Slab (1 rib)	30700	38×10^6	55	7.5	8.0×10^{-6}

Table 1: Section properties of composite slab in x and y directions

temperatures. Initially the bowing is fully restrained due to the continuity of the longitudinal composite beam over the primary beams into the adjacent compartment. This produces a fixed end like condition and generates uniform hogging moments in the composite section (tension in concrete and compression in steel). The extra compression added to the compression generated by the expansion of the steel secondary beam leads an early local buckling of the secondary beam bottom flange [4]. The result is the beginning of the development of a hinge mechanism near the column for the longitudinal composite section. Further heating produces relatively lower compressions (compared to before buckling) and deflections increase faster. A simple model that may be used for the test from the point when local buckling occurs is shown in Figure 3, where no rotational restraint has been assumed.

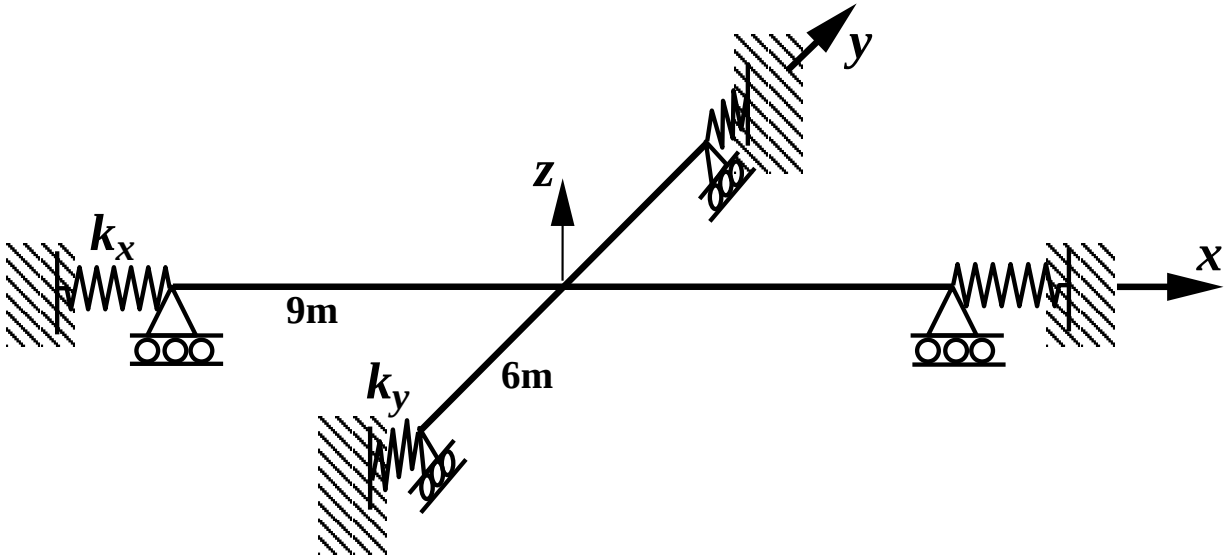

Figure 3: Analytical model of restrained beam test

The longitudinal springs (of stiffness k_x) represent the axial stiffness ($\frac{EA}{l}$) of the cold composite section in the adjacent compartment which provides the main restraint to the expanding composite beam. Another mechanism of restraint is the shear and flexure stiffness of the slab orthogonal to the expanding composite beam. Further restraint may be available from the in-plane shear resistance of the cold slab adjacent to the compartment. Figure 4 shows these mechanisms in a schematic manner. The stiffness provided by these mechanisms is orders of magnitude greater than that provided by the column, therefore any restraint provided by the column can be neglected in an 'order-of-magnitude' calculation such as this. The same kind of assumption are used to estimate the restraint in the transverse direction for the stiffness k_y.

To estimate the translational spring stiffness k_x, we can use the following expression,

$$k_x = \frac{E_s A_x}{L_x} + \left(\frac{f \frac{L_y}{2}}{2 G_c A_y} + \frac{L_y^3}{48 E I} \right)^{-1} \tag{1}$$

where, E_s and E_c are the moduli of elasticity of steel and concrete. A_x is the transformed area of the composite beam in the adjacent bay (see Figure 4 and Table 1) and A_y is an estimate of the area of orthogonal slab providing shear and bending restraint to the compartment. G_c is the shear modulus of concrete (approximately 3.1 kN/mm2 for a Poisson's ratio of 0.2), f is the form factor (assumed to be 1.2 as for a rectangular section). Assuming a 3m width of orthogonal slab the value of k_x can be estimated to be approximately 400 kN/mm. This is clearly a crude calculation, and a number of effects have been ignored such as the stiffness of steel beam and column framing across the impinging composite beam. However, it is sufficient to obtain a rough estimate of this value for the purposes of this analysis.

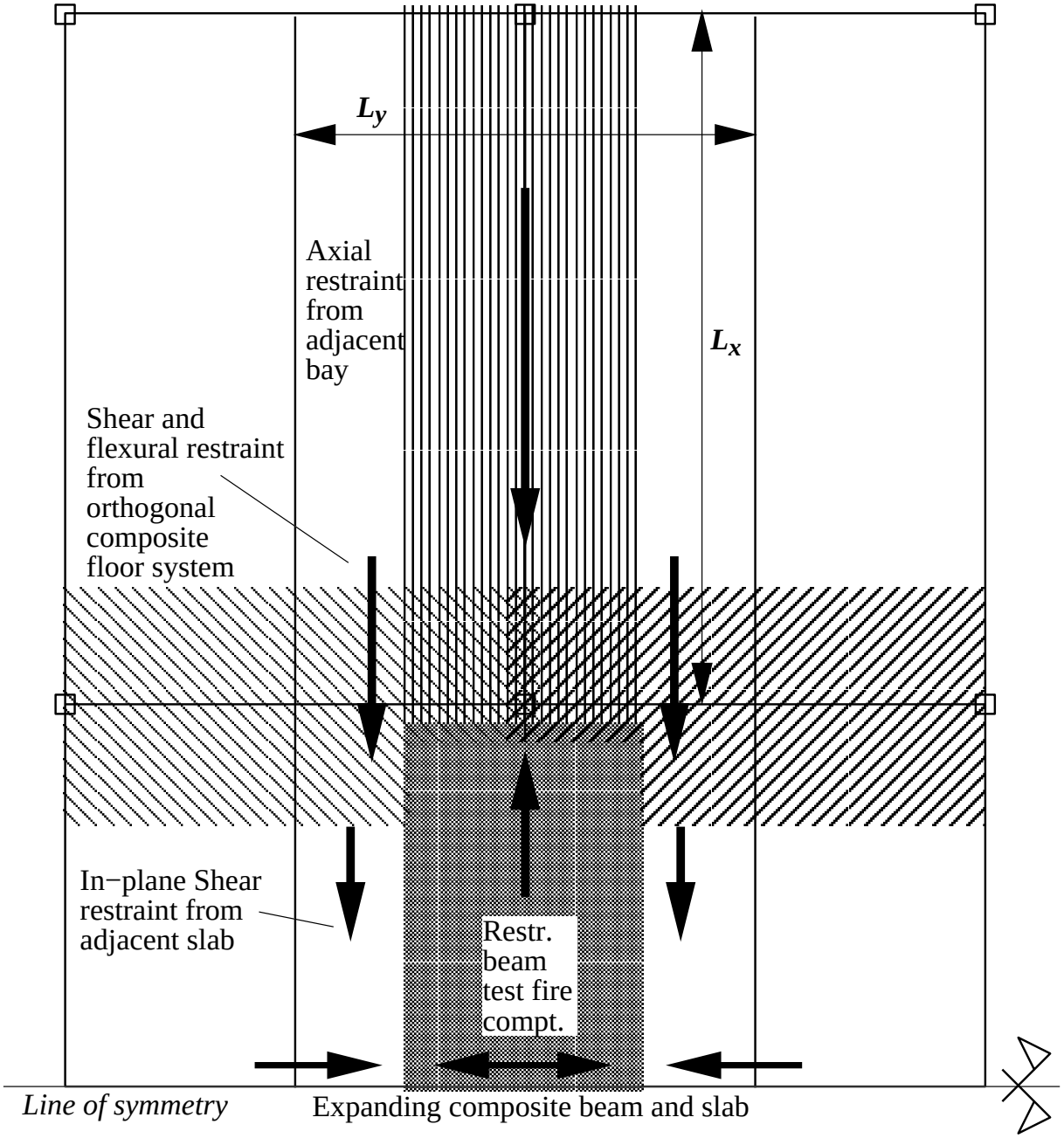

Figure 4: Restraint mechanisms around and internal fire compartment

For the member in the transverse direction, the width of middle 4 ribs (1.2m) has been assumed. This is the most effective part of the transverse slab in interacting with the longitudinal composite beam in terms of compatibility considerations. The spring stiffness k_y is also estimated as approximately 400 kN/mm.

2.2 Estimation of equivalent temperature effects on the model

The geometry of the simple model including the boundary restraints were determined in the previous section. The issue of the equivalent thermal loading that must be applied to the members is also not straightforward. A procedure has been developed based upon ideas used in estimating the effects of thermally induced stressed in bridge decks [5]. Figure 5 shows a general composite

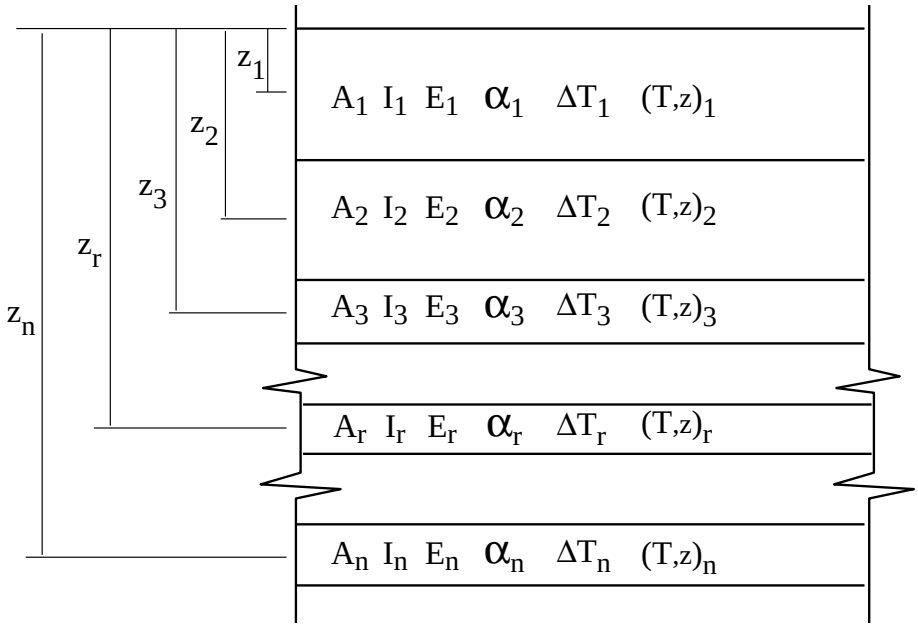

Figure 5: A general composite section divided into *n* slices

section with the indicated properties and temperature conditions, as defined by a uniform temperature increment $\Delta T, r$ and a through depth thermal gradient $T_{,z}$ for a given slice. If the beam that the section belongs to is fully restrained (both end translations and end rotations) then each slice will have a force and moment associated with it, defined as,

$$F_r = E_r A_r \alpha_r \Delta T_r = E_r A_r (\varepsilon_T)_r = E_{\max} \hat{A}_r (\varepsilon_T)_r \tag{2}$$

and,

$$M_r = E_r I_r \alpha_r (T_{,z})_r = E_r I_r \phi_r = E_{\max} \hat{I}_r \phi_r \tag{3}$$

It is convenient to write the above quantities using a transformed area (by defining modular ratios m_r based on the highest modulus in the composite), this is what $\hat{A}_r$ and $\hat{I}_r$ represent. The resultant force $\bar{F}$ and resultant moment $\bar{M}$ can now be determined from,

$$\bar{M} + \bar{F}\bar{z} = \sum F_r z_r + \sum M_r \tag{4}$$

where, $\bar{z}$ is the centroid of the composite. This If the total (transformed) area and second moment of area of the composite are denoted by $\bar{A}$ and $\bar{I}$, then the equivalent expansion $\bar{\varepsilon}_T$ and curvature $\bar{\phi}$ can be written as,

$$\bar{\varepsilon}_T = \frac{\bar{F}}{E_{\max} A} \tag{5}$$

and,

$$\bar{\phi} = \frac{\bar{M}}{E_{\max} I} \tag{6}$$

This procedure can also be use to determine the thermally induced strains and stresses in a composite beam. This can be done by releasing the restraint applied to determine the resultant force and moment in the composite. Which, of course, is the same as applying the negatives of $\bar{F}$ and $\bar{M}$, bringing the restraint forces to zero. This is illustrated using an example in Figure 6. The total strain distribution in the beam can then be determined by,

$$\varepsilon(z) = \bar{\varepsilon}_T + (z - \bar{z})\bar{\phi} \tag{7}$$

and the stresses are,

$$\sigma(z) = \frac{E_{\max}}{m_r}\left[(\varepsilon_T)_r + (z - z_r)\phi_r + \varepsilon(z)\right] \tag{8}$$

Figure 6 shows the distributions of stresses and strains computed using this procedure for a simple example of a composite beam.

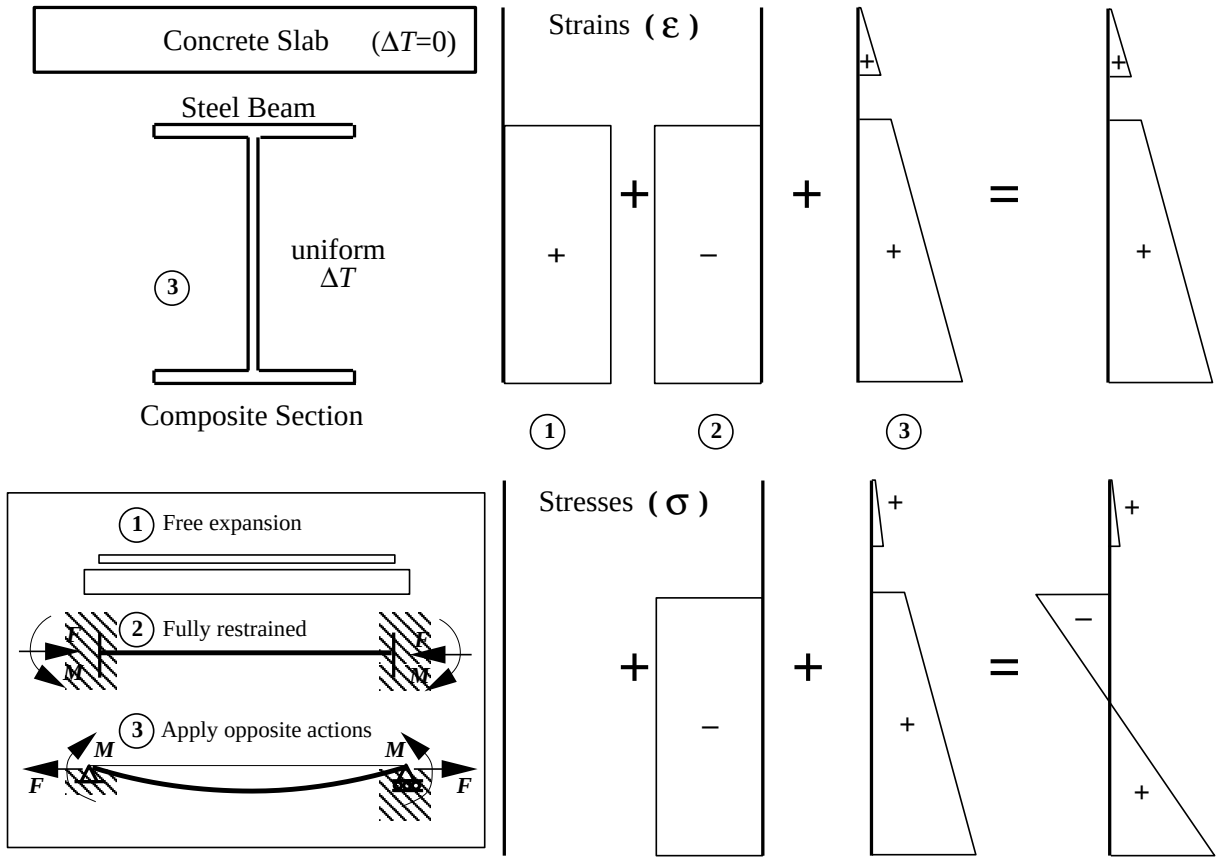

Figure 6: Analysis of thermal actions on a composite beam

For the restrained beam model of Figure 3 equivalent temperatures and gradients were calculated for three different reference temperature states of the steel beam, for both directions (longitudinal and transverse), using the procedure outlined above. The results are tabulated in Tables 2 and 3, along with other data that will be used in the analysis. It may be noted that the temperature distributions in the real structure are complicated by the effect of the ribs, and therefore appropriate averages have been used in these calculations. λ denote slenderness ratio, and $\bar{z}$ denotes the depth of centroid of the transformed composite sections, subscripts *x* and *y* have been used to indicate longitudinal or transverse directions. Most other quantities in the tables should be self-explanatory.

Steel Temp.	E_s kN/mm^2	E_c kN/mm^2	A_x mm^2	I_x mm^4	$\bar{z}_x$ mm	λ_x	ΔT_x °C	$(T_{,z})_x$ °C/mm
150°C	200	7.5	10900	250×10^6	148.0	60	80	0.5
500°C	100	7.5	16800	300×10^6	108.5	67	260	1.6
800°C	0	7.0	124000	48×10^6	30.0	450	240	5.0

Table 2: Properties of composite slab in x direction at different temperatures

Steel Temp.	E_c kN/mm^2	A_y mm^2	I_y mm^4	$\bar{z}_y$ mm	λ_y	ΔT_y °C	$(T_{,z})_y$ °C/mm
150°C	7.5	30700	38×10^6	55.0	170	-	-
500°C	7.5	30000	37×10^6	54.0	170	85	1.4
800°C	7.5	19200	17×10^6	39.0	200	250	4.8

Table 3: Properties of composite slab in y direction at different temperatures

2.3 Analysis

The above data (given in Tables 2 and 3) will now be used to analyse the restrained beam test at various stages during the fire.

2.3.1 At steel beam reference temperature of 150°C

The equivalent mean temperature and gradient for the composite member in the longitudinal direction is given as 80°C and 0.5°C/mm. This is calculated according to the procedure outlined earlier, after applying a uniform temperature of 150°C to the steel beam and zero to the concrete slab (as shown in Figure 6). This leads to a thermal 'expansion' strain (ε_T) and a 'contraction' strain (ε_ϕ) of,

$$\varepsilon_T = 7.1\times10^{-4}$$

and

$$\varepsilon_\phi = 8.1\times10^{-5}$$

These values have been modified for an 8m heated length (against a 9m overall length). The curvature

$$\phi = \alpha T_{,z} = 5\times10^{-6}$$

If the composite beam is assumed to be fully restrained (not an reasonable assumption early on in the fire), then the The stress in the bottom fibre of the beam can be calculated to be

$$\sigma(z) = E_s\varepsilon_T - E\phi(z-\bar{z}) = 200(-7.1\times10^{-4} - 5\times10^{-6}(434-148)) \simeq 400.0\text{MPa}$$

This stress suggests clearly that the beam bottom flange has buckled or yielded earlier than this temperature (given the reported yield strength of the grade 275 steel used is between 291 to 318 MPa). It is important to note that this early local buckling event is a combination of the thermal expansion and the thermal bowing effects acting together. If there was no gradient, the stress in the bottom fibre would be only 160 Mpa (due to restrained thermal expansion).

Effect of restraint

The above calculation for steel bottom flange stress assumed a rigid restraint. If we assume the end restraint to be elastic and of the value estimated earlier (400kN/mm), then the force in the beam is calculated to be,

$$F = \frac{E_sA_x(\varepsilon_T - \varepsilon_\phi)}{1+\frac{E_sA_x}{k_xL_x}} \simeq 850\text{kN}$$

The same value for a rigid restraint is 1370kN. This reduces the steel beam bottom flange stress to approximately 340MPa, which is still greater than 318MPa, so the conclusion about local buckling does not change. Furthermore the force of 850kN is very low as should be clear from the following. The force of 850kN against a spring of stiffness 400kN/mm should produce an end displacement of over 2mm. However the reported column displacement from the test is near 0.3mm at this beam temperature. This suggests that the actual restraint must be much greater than 400 kN/mm. The force of 850kN is however not that far from the rigid restraint force of approx. 1370kN (when the end displacement would be zero). Therefore the end displacement quantity is clearly very sensitive to the magnitude of end restraint however the axial compression force in the composite is much less sensitive. These forces compare well with results from finite element models reported in [3], as being between 1700kN to 2000kN (the lower values are from two grillage models and the higher value from a model using shell finite elements). There are very good reasons for the low estimate obtained here and will become clear in the next section on deflections. For further calculations a rigid restraint will be assumed in both directions. The magnitude of the forces calculated above can be appreciated relative to the Euler buckling force for the steel beam, 2000kN and that for the composite, 6000kN.

Deflection

As the beam is clearly in the pre-buckling mode, the thermally induced deflections will only consist of the contribution from thermal bowing. The midspan deflection 'δ' can be calculated by using one of the formulas from [4],

$$\delta = \frac{2L_x}{\pi}\sqrt{\varepsilon_\phi} = 52\text{mm}$$

This value is reduced by considering the effect of compatibility with the member spanning in the transverse (y) direction. At the steel temperature of 150°C the transverse member has negligible temperature increase and therefore this is neglected. This member resists the downward deflection of the longitudinal composite beam in flexure or by developing membrane tension. Considering flexure only here, the spring stiffness of flexural member against a point load at midspan can be written as,

$$k = \frac{48EI}{L^3}$$

which give the stiffnesses of the longitudinal (k_l) and the transverse (k_t) members as 3.3kN/mm and 0.25kN/mm respectively. If now the true deflection (after applying compatibility) is Δ, then we can write,

$$k_l(\delta - \Delta) = k_t\Delta$$

which gives,

$$\Delta = \frac{\delta k_l}{k_l + k_t} = 48\text{mm}$$

This deflection is considerably higher than the one in the test at this point (approx 30mm). The reason is that the simple model chosen here does not provide anywhere near the true stiffness in the transverse direction. The results should therefore improve if a much stronger transverse member is chosen (say 10-15 ribs instead of 4). This also provides the explanation for the low axial force in the composite as calculated earlier. Because as much thermal expansion is not converted to displacement (strains) it naturally goes towards increasing the compressive forces (stresses).

Despite the above conclusion about the transverse member being less stiff, this model was chosen here is to illustrate another effect! The force transferred to the transverse member caused by the composite beam deflection acts as point load P on its midspan,

$$P = k_t\Delta = 12\text{kN}$$

The tensile stress in the lowest fibre of this member can now be calculated (using the data in Table 3) to be 9Mpa. This is clearly very high (given that the concrete compressive strength is 35-40Mpa), and suggests that tensile cracking would occur at an early stage, leading to tensile membrane forces developing in the middle ribs. Two of the three models in [3] predict this, the one that shows compression in the middle rib at the early stages used higher temperatures in the concrete (using a linear evolution from minimum to maximum temperature). It should be noted that this is just an illustration of a point and does not mean that tensile cracks may have appeared in the ribs in the actual test. Remember the model here grossly underestimates the stiffness in the transverse direction (only 4 ribs out of 30 considered and reinforcement and steel decking not included for simplicity). For the calculations from here on, the transverse member will be assumed to be made up of 10 ribs (middle third).

2.3.2 At steel beam reference temperature of 500 °C

First considering the longitudinal direction (using data from Table 2),

$$\varepsilon_T = 2.3 \times 10^{-3}$$

and

$$\varepsilon_\phi = 8.34 \times 10^{-4}$$

therefore,

$$\varepsilon_T - \varepsilon_\phi = 1.48 \times 10^{-3}$$

buckling strain ($\frac{\pi^2}{\lambda^2}$) 2.2×10^{-3}, which is greater than $\varepsilon_T - \varepsilon_\phi$, so the composite beam is in a pre-buckling regime and some of the thermal expansion is going towards increasing deflections but most towards increasing stresses. The bowing related strain (ε_ϕ) gets converted to deflection completely, which is approximately 165mm.

Now considering the transverse direction (using data from Table 3),

$$\varepsilon_T = 3.4 \times 10^{-4}$$

and

$$\varepsilon_\phi = 1.23 \times 10^{-4}$$

therefore,

$$\varepsilon_T - \varepsilon_\phi = 2.17 \times 10^{-4}$$

This compressive strain is available to offset tensile strains induced by the compatibility deflections. The bowing related strain produces a deflection of 42mm. The balance (165-42) must be adjusted using compatibility. The flexural stiffness of the longitudinal composite beam k_l is 2.0kN/mm, while that of the transverse beam (now 10 ribs) is 2.5 kN/mm (note that this will be further enhanced by tensile membrane action). The true deflection therefore is,

$$\Delta = \frac{\delta k_l}{k_l + k_t} + 42 = \frac{123 * 2.0}{2.0 + 2.5} + 42 = 97\text{mm}$$

This compares well with the test deflection of approximately 120mm. These values are extremely sensitive to the estimates of transverse stiffnesses. It is very difficult to obtain a good representation of the stiffness in a simple model like this, particularly in the region near the columns, where the slope of the composite beam will be reduced by the ribs which are in compression and are very stiff due to a pre-stressing like effect. Also in this model no account has been taken of the reinforcement or the steel decking. Furthermore, the use of the flexural stiffness here is highly artificial, as when the stresses due to moment on the transverse member caused by the reaction it provides to the

deflecting composite beam are analysed, the extreme fibre tensile stress value is calculated to be approximately 37MPa! There is some flexural stiffness available in the transverse direction but clearly not as much as assumed here, however there is considerable membrane stiffness available, which is a lot more difficult to estimate accurately as it rises exponentially with the deflection (membrane stiffening). Another calculation shows that for a deflection of 55mm the mean tensile strain caused in the transverse member is 2.07×10^{-4} which is less than the residual compressive strain above ($\varepsilon_T - \varepsilon_\phi = 2.17 \times 10^{-4}$, based upon rigid restraint assumption). This is perhaps a more realistic interpretation as it is geometrically consistent in contrast to the calculation of flexural stress (based on small displacement theory). These calculation clearly illustrate that the potentially large deflections in the composite beam are arrested by the orthogonal slab and the additional load this imposes on the slab is considerably greater than the imposed loads and cannot be carried only by the conventionally assumed flexure and shear mechanisms and tensile membrane action is clearly present.

The axial compression force now in the composite member can be calculated using the compression strain calculated earlier ($\varepsilon_T - \varepsilon_\phi$), enhanced by the 'rebound' (of 165-97=68 mm) caused by the resistance to deflection. This gives a total compressive strain of 1.62×10^{-3}, leading to a compressive force of 2700kN. This can be compared with the forces from the computer analyses reported in [3] as, 2300kN for the ABAQUS grillage model and 3200 from the ABAQUS shell model and the ADAPTIC grillage model. Again, considering the crudeness of the analysis here, the comparison is fairly respectable.

2.3.3 At steel beam reference temperature of 800°C

At this stage the steel beam has effectively lost all strength. The values of expansion and bowing strains are now, for the longitudinal direction,

$$\varepsilon_T = 1.7 \times 10^{-3}$$

and

$$\varepsilon_\phi = 5.2 \times 10^{-3}$$

therefore,

$$\varepsilon_T - \varepsilon_\phi = -3.5 \times 10^{-3}$$

and for the transverse direction,

$$\varepsilon_T = 1.0 \times 10^{-3}$$

and

$$\varepsilon_\phi = 1.1 \times 10^{-3}$$

therefore,

$$\varepsilon_T - \varepsilon_\phi = -1.0 \times 10^{-4}$$

These values suggest that the problem is now completely dominated by thermal bowing effects. The deflections in the two directions now consist of thermal expansion related deflection (which is 235mm in the longitudinal direction and 125mm in the transverse direction) and additional deflections caused by thermal bowing. The thermal bowing related deflection will be much larger in the longitudinal direction (as the absolute value of $\varepsilon_T - \varepsilon_\phi$ is 35 times greater in this direction) if the beam ends are laterally unrestrained (of the order of 300mm). However as the beam ends are restrained against translation, the deflections (ignoring compatibility for now) are approximately 70mm (assuming bowing only), with a net tensile force in the longitudinal composite beam. The actual midspan deflection in a laterally restrained beam subjected to both thermal expansion and thermal bowing is dependent upon the relative values of axial and flexural stiffness of the beam. A

slender beam (of low flexural stiffness - such as the slab in isolation as considered here) does not have sufficient flexural stiffness to overcome the tensile axial stiffness and develop curvature (or 'bow') as much as a stocky beam (with relatively large flexural stiffness) would. Therefore bowing deflection will be much lower in slender beams (as here) than in stocky composite beams. In the extreme the actual deflection in a very slender beam can be slightly 'lower' with combined thermal expansion and thermal bowing than the deflection caused only by thermal expansion. This is due to the change in slope caused by bowing induced tensile forces at the ends.

These deflections are restrained by a relatively much stiffer transverse slab now (as the steel beam has gone out of the picture). This will result in very little actual growth in the deflections (the actual deflection at 800 °C in the restrained beam test is approximately 225mm). The arrest of deflection growth will lead to the development of compression in the longitudinal slab. This compression can be estimated by the taking an appropriate proportion of the restrained thermal bowing related strain ($\varepsilon_T - \varepsilon_\phi = -3.5 \times 10^{-3}$) based upon an estimate of the relative stiffness of the longitudinal and transverse members and multiplying by the axial stiffness of the restrained longitudinal member. Using approximately two thirds of the value of $\varepsilon_T - \varepsilon_\phi$ a compression force of 2000kN is obtained, which is within the range of figures achieved by various computer models [3]. Tension clearly exists in the orthogonal transverse member that restrains the deflections of the longitudinal slab.

The above analysis is as yet very crude and a number of other factors such as tensile and compressive membrane stiffnesses in the two directions and their interactions with the flexural stiffness needs to be determined more accurately to refine the above calculations. Even so, the description of the behaviour from this analysis is no different from that obtained by sophisticated computer models.

3 Conclusions

Simple calculations have been presented, based upon the application of some fundamental structural mechanics principles to estimate the forces and displacements in the Cardington restrained beam test and compare the structural behaviour so observed both quantitatively and qualitatively with the test and more sophisticated computational analysis. It is clear that the calculations do provide a means of obtaining order-of-magnitude type assessments of the response of a real structure subjected to fire. Both qualitative and quantitative agreement was found. This however is still a very early development and considerable refinements can be made to the calculations as presented, such as better estimation of the restraint effects and better idealisation of the structure. Also a simple means of calculating the of tensile membrane stiffness of slabs will be useful. Highly nonlinear problems such as this (in terms of both material and geometry) are clearly history dependent and a simple scheme of approximating this is also needed. The method as it is, is still valuable if used to check calculations from more sophisticated methods and perhaps for preliminary design calculations in a consulting office. However, the greatest use by far of the ideas presented here is in helping to understand the mechanics of structural behaviour in fire.

References

[1] J.M.Rotter, A.M.Sanad, A.S.Usmani, and M.Gillie. Structural performance of redundant structures under local fires. In *Interflam'99, 8th International Fire Science and Engineering Conference*, pages 1069–1080, Edinburgh, Scotland, 29 June - 1 July 1999.

[2] A.S.Usmani and J.M.Rotter. Fundamental principles of structural behaviour under thermal effects. Technical Report PIT/TM2, School of Civil and Environmental Engineering, University

of Edinburgh, 2000. Submitted to DETR(UK) as part of the final report for the PIT project *Behaviour of Steel frame Structures under fire conditions*.

[3] A.S.Usmani, M.A.O'Connor, J.M.Rotter, A.Y.Elgahzouli, D.D.Drysdale, A.M.Sanad, M.Gillie, and S.Lamont. Final report of detr pit project: Behaviour of steel framed structures under fire conditions. Technical report, University of Edinburgh, 2000.

[4] J.M.Rotter and A.S.Usmani. Fundamental principles of structural behaviour under thermal effects. Copenhagen, Denmark, June 2000. Ist International Workshop, Structures in Fire.

[5] R.P.Johnson and R.J.Buckby. *Composite structures of steel and concrete - Volume 2: Bridges*. Collins, London, U.K., 1986.